

Supplemental Methods and Figures

PET data acquisition

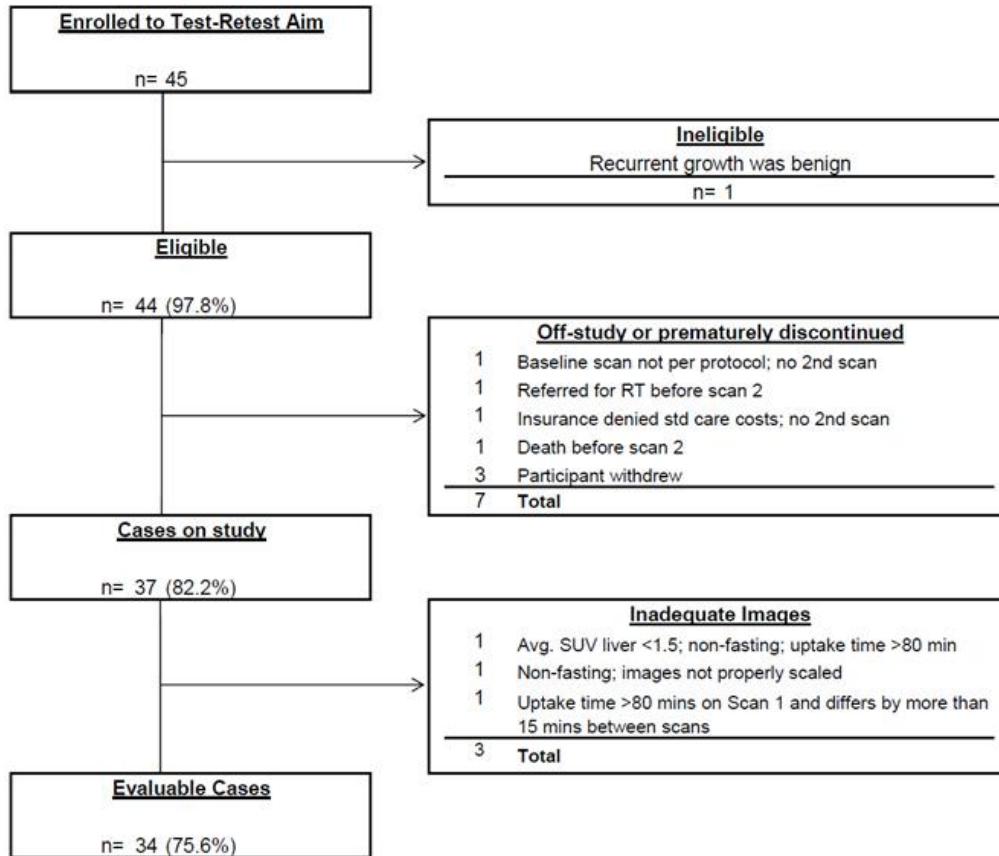
Participants fasted for at least four hours prior to ^{18}F -FDG injection. Upon arrival at the PET facility, patient body weight and blood glucose level were measured. ^{18}F -FDG was administered via an intravenous line to minimize the risk of paravenous infiltration. The amount of radioactivity was adjusted according to the body weight of the patient as recommended by the scanner manufacturer.

The exact time of calibration of the dose and precise time of injection were recorded to permit correction of the administered dose for radioactive decay. In addition, the dose remaining in the tubing or syringe was measured, recorded, and subtracted from the injected radioactivity. PET imaging was scheduled to start 50-70 minutes after ^{18}F -FDG injection. The time between the injection and start of the second PET scan was to be matched as closely as possible to that of the first scan (less than 10 minutes difference in radiotracer uptake times). A low-dose CT scan was acquired for attenuation correction and anatomical localization of findings in the PET scan.

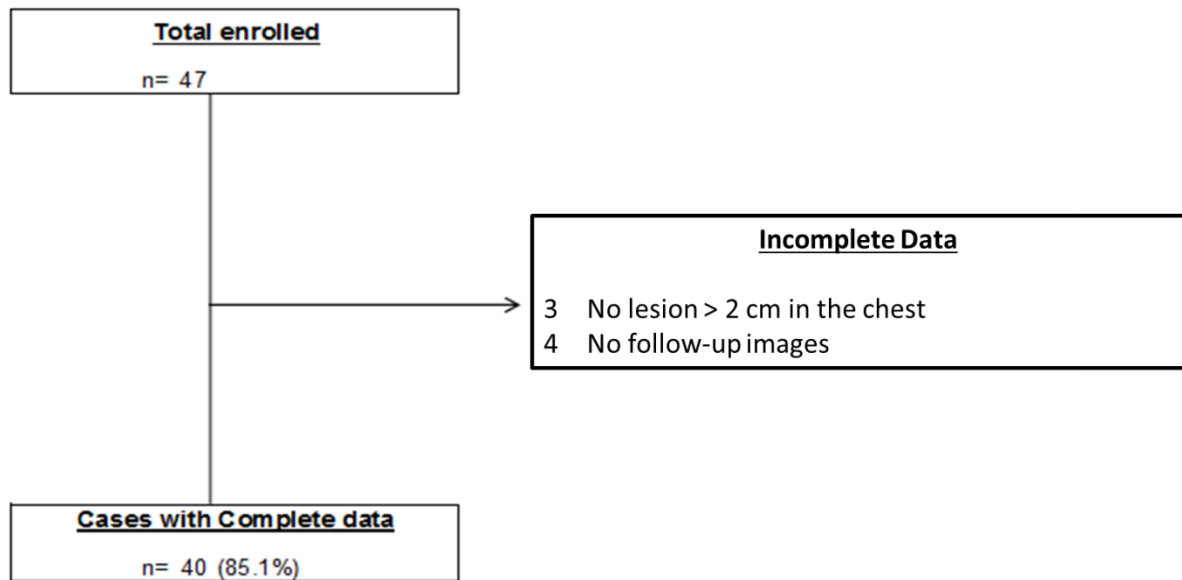
Typical acquisition parameters: kVp = 120; effective mAs = 30-80 (patient-dependent); gantry rotation time \leq 0.5 seconds; maximum reconstructed width = 3-5 mm without overlap; minimum reconstruction diameter = outer arm to outer arm. No iodinated contrast was administered for the CT study to avoid potential interference with SUV measurements (1). The craniocaudal field of view of the CT scan ranged from the mid-thighs to the base of the skull. Arm positioning was the same for the CT and PET scan, typically above the head unless this position was not tolerated by the patient. The CT scans were performed during "shallow breathing." No respiratory gating was applied.

After the CT scan, a PET scan covering the same field of view was performed (starting at the mid-thighs). The number of bed positions and acquisition time per bed position were scanner-specific. Typical parameters were six bed positions and an acquisition of 2-5 minutes per bed position. The PET data were corrected for dead time, scatter, random coincidence events, and attenuation using standard algorithms provided by the scanner manufacturers. Image reconstructions were performed in accordance with manufacturer recommendations and as specified in the ACRIN qualification of the PET/CT scanner. The baseline and follow-up studies were performed on the same PET/CT scanner or on scanners of the same model if multiple ACRIN-qualified scanners were used at a participating PET facility. The baseline and follow-up PET/CT scans were performed within one week for all patients. A clinical PET/CT scan acquired for tumor staging as part of the routine clinical care of the patient could be used for comparison with the follow-up research PET/CT study if it was acquired per protocol and performed on an ACRIN-qualified PET/CT scanner.

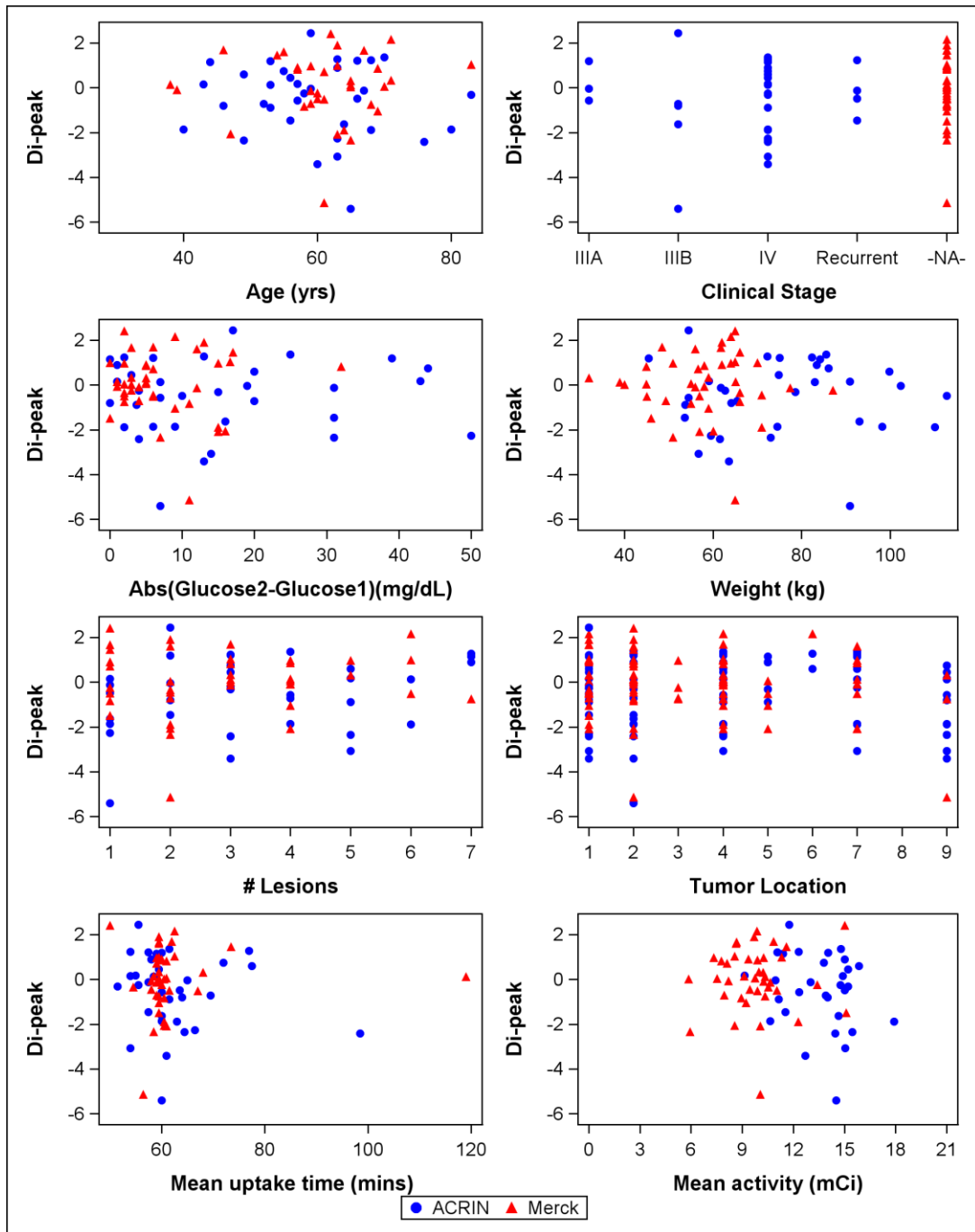
1. Brix G, Lechel U, Glatting G, et al. Radiation exposure of patients undergoing whole-body dual-modality 18F-FDG PET/CT examinations. *J Nucl Med.* Apr 2005;46(4):608-613.



Supplemental Figure 1. STARD Flowchart Showing Development of Analysis Set for ACRIN 6678. In one patient with suspected recurrence, malignancy was not confirmed. In one patient, the baseline scan was not performed according to protocol, and no second PET/CT was performed. In one patient, radiotherapy was started prior to the second PET/CT, one patient did not undergo the second PET/CT because of logistical problems, and one patient died prior to the planned second PET/CT study. Three patients withdrew from the study after the baseline scan. Three additional patients were excluded because of inadequate images (either due to incorrect radiotracer uptake time or lack of fasting prior to FDG injection).



Supplemental Figure 2. STARD Flowchart Showing Development of Analysis Set-MERCK MK-0646-008. In three patients, there was no measurable target lesion in the chest, so these cases were excluded from further analysis. In four additional patients, no follow-up imaging was available.



Supplemental Figure 3. Scatter plots showing the correlation between various clinical parameters and the variability of SUVpeak measurements. Clinical stage is not available for individual Merck participants, though all were stage IIIB, IV, or recurrent. Tumor location plot includes target and additional lesions; the maximum number of lesions that could be reported was seven.

Supplemental Figure 3 legend for lesion location.

Value	Tumor location
1	Right or left upper lobe
2	Right or left lower lobe or right middle lobe
3	Pleura
4	Lymph nodes
5	Liver
6	Adrenal glands
7	Bone (marrow)
8	Brain
9	Other location

Table 1. Spearman correlation coefficients between test and retest measurements of tumor ¹⁸F-FDG uptake.

Parameter		N	Spearman Correlation
Liver	SUVmean-A	34	0.826
	SUVmean-M	40	0.658
	SUVmean-P	74	0.740
Tumors	SUVmax-A	34	0.918
	SUVmax-M	40	0.905
	SUVmax-P	74	0.924
	SUVpeak-A	34	0.910
	SUVpeak-M	40	0.893
	SUVpeak-P	74	0.915
	aSUVmax-A	34	0.943
	aSUVmax-M	40	0.851
	aSUVmax-P	74	0.912
	aSUVpeak-A	34	0.952
	aSUVpeak-M	40	0.813
	aSUVpeak-P	74	0.911

SUVmean, average SUV in liver; SUVmax, maximum SUV of target lesion; SUVpeak, SUV peak of target lesion; aSUVmax, maximum SUV averaged across all lesions within an individual patient; aSUVpeak, SUV peak averaged across all lesions within an individual patient. Results of the ACRIN trial are denoted with -A, those from the Merck trial with -M, and those from pooled ACRIN and Merck data with -P.

Supplemental Table 2. Within-subject coefficients of variation (wCV) for relative SUV changes

Parameter	wCV(%)
SUVmax-A	12.1
SUVmax-M	13.2
SUVmax-P	12.7
<hr/>	
SUVpeak-A	12.6
SUVpeak-M	16.5
SUVpeak-P	15.0
<hr/>	
aSUVmax-A	11.9
aSUVmax-M	12.4
aSUVmax-P	12.3
<hr/>	
aSUVpeak-A	10.9
aSUVpeak-M	14.5
aSUVpeak-P	13.1
<hr/>	

Supplemental Table 3. Participating sites and site PIs for the ACRIN 6678 trial

Site Name	PI Name	Location
Boston Medical Center	Rathan Subramanian, MD, PhD	Boston, MA
Cedars-Sinai Medical Center	Peter Julien, MD	Los Angeles, CA
Fox Chase Cancer Center	Michael Yu, MD	Philadelphia, PA
Georgia Regents University	Haydn Williams, MD	Augusta, GA
H. Lee Moffitt Cancer Center and Research Institute	Edward Eikman, MD	Tampa, FL
Hospital of the University of Pennsylvania	Drew Torigian, MD	Philadelphia, PA
Icahn School of Medicine at Mount Sinai	Lale Kostakoglu, MD	New York, NY
Nevada Cancer Institute	Delva Deauna-Limayo, MD	Las Vegas, NV
Peking Union Medical College Hospital	Zhaohui Zhu, MD	Beijing, China
Piedmont Hospital	Sabah Tumeah, MD	Atlanta, GA
Scottsdale Medical Imaging, LTD	Ronald Korn, MD, PhD	Scottsdale, AZ
University of North Carolina	Amir Khandani, MD	Chapel Hill, NC
University of Southern California	Christopher Lee, MD	Los Angeles, CA
Virginia Commonwealth University Health System	Robert Halvorsen, MD	Richmond, VA
Wake Forest University	Caroline Chiles, MD	Winston-Salem, NC
Washington University School of Medicine	Barry A. Siegel, MD	St. Louis, MO
Wayne State University	Anthony Shields, MD, PhD	Detroit, MI

Supplemental Table 4. Staff at ACRIN headquarters and at Brown University's Biostatistical and Data Management Center.

Name	Role/Department
Donna Hartfeil, RN, BSN	Project Management
Leslie Sears, LPN	Administration
Laura Hill, BS	Data Management
Jamella Knots-Miller, BS, CCDM	Data Management
James Gimpel, RT (R) (MR)	Imaging
Kesha Smith, RT (R) (MR)	Imaging
Adam Opanowski, CNMT, PET, NCT, RT (N)	Imaging
Maria Oh, MS	Protocol Development and Regulatory
Josephine Schloesser, BA, RT (R) (M) (QM)	Regulatory
Chris Steward, BS, RT (R) (CV)	Regulatory
Nancy Fredericks, MA	Communication
Erin Greco, MS	Statistics

The authors also appreciate the expert help of Leah Bassity in editing the manuscript.